An Electric-Field-Reinforced Hydrophobic Cationic Sieve Lowers the Concentration Threshold of Water-In-Salt Electrolytes

Anxing Zhou, Jinkai Zhang, Ming Chen, Jinming Yue, Tianshi Lv, Binghang Liu, Xiangzhen Zhu, Kun Qin, Guang Feng,* and Liumin Suo*

High-concentration water-in-salt (WIS) electrolytes expand the stable electrochemical window of aqueous electrolytes, leading to the advent of high-voltage (above 2 V) aqueous Li-ion batteries (ALIBs). However, the high lithium salt concentration electrolytes of ALIBs result in their high cost and deteriorate kinetic performance. Therefore, it is challenging for ALIBs to explore aqueous electrolytes with appropriate concentration to balance the electrochemical window and kinetic performance as well as the cost. In contrast to maintaining high concentrations of aqueous electrolytes (>20 m), a small number of hydrophobic cations are introduced to a much lower electrolyte concentration (13.8 m), and it is found that, compared with WIS electrolytes, ALIBs with these concentration-lowered electrolytes possess a compatible stable electrochemical window (3.23 V) and achieve better kinetic performance. These findings originate from the added cations, which form an electric-field-reinforced hydrophobic cationic sieve (HCS) that blocks water away from the anode and suppresses the hydrogen evolution reaction. Meanwhile, the lower electrolyte concentration provides significant benefits to ALIBs, including lower cost, better rate capability (lower viscosity of 18 cP and higher ionic conductivity of 22 mS cm^{-1} at 25 °C), and improved low-temperature performance (liquidus temperature of −10.18 °C).

1. Introduction

Aqueous electrolytes are sustainable for electrical energy storage because of the safety, environmental friendliness, and low cost of water solution.[1] However, the narrow electrochemical window of aqueous electrolytes lowers the output voltage and cycle life of aqueous batteries, such as aqueous Li-ion

batteries (ALIBs), hindering their application.[2] Furthermore, compared with the cathode, it is more challenging for the anode to suppress the hydrogen evolution reaction (HER) because the lithiation potential of most anode materials is lower than that of the HER, resulting in cycling fading.[3] Considering that the HER occurs on the interface of the anode, interfacial properties are the critical factors, particularly under the electric field coming from the anode, because water-rich domains preferably form on the anode interface owning to the occupation of ion–water solvation in the inner Helmholtz layer.[4] Recently, water-in-salt (WIS) electrolytes have been proposed and successfully expanded the electrochemical window of aqueous electrolytes by over 3 V through the manipulation of the interphase chemistry and interface structure,[5] leading to the advent of ALIBs above 2 V.[5b,6] These studies indicate that interfacial properties are clearly the determining and dominant factors behind achieving a stable aqueous electrolyte in real batteries.[3b]

Developing various WIS electrolytes, many efforts that take the salt concentration as the crucial variable for the development of high-concentration aqueous electrolytes (such as water-in-bisalt, WIBS)[5b,7] that indeed refresh the record of the concentration. However, limited by the lithium reserve on land, the rapid increase of lithium consumption may result in a lack of lithium supply.[8] In this scenario, a high salt

A. Zhou, J. Yue, T. Lv, B. Liu, X. Zhu, K. Qin, L. Suo
Beijing Advanced Innovation Center for Materials Genome Engineering, Key Laboratory for Renewable Energy
Beijing Key Laboratory for New Energy Materials and Devices
Beijing National Laboratory for Condensed Matter Physics
Institute of Physics
Chinese Academy of Sciences
Beijing 100190, China
E-mail: suoliumin@iphy.ac.cn

The ORCID identification number(s) for the author(s) of this article can be found under https://doi.org/10.1002/adma.202207040.

A. Zhou, J. Yue, T. Lv, B. Liu, X. Zhu, K. Qin, L. Suo
Center of Materials Science and Optoelectronics Engineering
University of Chinese Academy of Sciences
Beijing 100049, China
J. Zhang, M. Chen, G. Feng
State Key Laboratory of Coal Combustion
School of Energy and Power Engineering
Huazhong University of Science and Technology (HUST)
Wuhan 430074, China
E-mail: gfeng@hust.edu.cn
L. Suo
Yangtze River Delta Physics Research Center Co. Ltd
Liyang 213300, China

**ADVANCED
SCIENCE NEWS**

www.advancedsciencenews.com

**ADVANCED
MATERIALS**

www.advmat.de

concentration is not appropriate and inevitably results in a high cost. What's more, poor kinetic and low-temperature performance due to high viscosity, low conductivity, and a high solid–liquid transition temperature further limit the application of high-salt-concentration electrolyte.[5b]

Therefore, it is still challenging to achieve an aqueous electrolyte with a wide electrochemical window and superior kinetic property with decreased concentration because lowering the salt concentration would exacerbate the HER problem on the anode interface.[1c,5a,7a,9] Inspired by the regulation of the interface structure to prevent water from the reaction,[10] we propose using hydrophobic cations to tune the interface on the anode side to suppress the HER. Specifically, under the electric field stemming from the anode, hydrophobic cations could accumulate on the anode, serving as a sieve (named hydrophobic cation sieve, HCS) that excludes the water from the interfacial region, resulting in the suppression of water decomposition. This conceptual HCS would make high salt concentration unnecessary for WIS electrolytes. Furthermore, considering the solvation effect of Li+,[11] when the concentration of the lithium salt reaches an appropriate concentration of 13.8 m, the molar ratio of Li+ to water becomes 1:4. At this molar ratio, Li+ ions in the electrolyte are sufficiently abundant to bind with all the water molecules so that almost no free water is left. Hence, the appropriate concentration electrolyte (ACE) of 13.8 m salt with HCS may achieve stability as high-concentration WIS electrolytes (>20 m).

In this work, tetraethylammonium+ (TEA+) is selected as the hydrophobic cation to demonstrate the concept of HCS. As revealed by molecular dynamics (MD) simulations, the more negative the polarization is, the more TEA+ ions in HCS-ACE (5 wt% TEA+ added to 13.8 m LiTFSI) accumulate on the anode to form a stronger HCS. Consequently, the more interfacial water molecules decrease, elaborating the electric-field-reinforced effect of HCS. It reveals for the first time that the added hydrophobic cations (TEA+) modulate the electronic double layer (EDL) on anode interface from the molecular perspective, and therefore lower the concentration of the aqueous electrolyte. Furthermore, the HCS-ACE can reach an electrochemical window of 3.23 V, comparable to WIBS electrolytes (28 m). Importantly, the salt concentration is significantly lowered with the aid of hydrophobic TEA+, so that the HCS-ACE costs much less while exhibiting excellent physical–chemical behaviors, including low viscosity (18 cP at 25 °C), high ion conductivity (22 mS cm−1), and a low liquid temperature (−10.18 °C), which are beneficial to improve the kinetics and temperature tolerance of ALIBs.

2. Result and Discussion

2.1. Constructing the Hydrophobic Cationic Sieve (HCS) on the Anode Surface

Theoretically, the coordination number of water molecules in the primary solvation shell of a solvated Li+ is four,[11] and then if only considering the effect of solvated Li+ on lowering water activity, the molar ratio of Li+ to water can be minimized to 1:4 (corresponding to a concentration of 13.8 m), so that all the water is possibly bounded with Li+ (**Figure 1**a). When the molar ratio of Li+ to water is less than 1:4, some water molecules will be in the secondary solvation sheath of Li+ and exist in a free

state.[4b] Such water molecules are unfavorable for the stable electrochemical window of the electrolyte[5a] (Figure 1a). Therefore, the relatively low concentration of 13.8 m LiTFSI (i.e., ACE) is selected as the base solution whose concentration is the minimum demand for Li+–water solvation. It is known that under the negative polarization, solvated Li+ prefers to occupy the interfacial region of the anode, resulting in the HER.[4a,b,d] To minimize the possibility of water molecules contacting the anode, a certain amount of tetraethylammonium trifluoromethanesulfonate (TEAOTF) is introduced into ACE. Driven by the electric field coming from the anode, the hydrophobic TEA+ cations accumulate to construct the HCS (Figure 1b). Because of the hydrophobicity and large size of TEA+, it has negligible hydration ability[10d] and inertness to the electrode.[7c] During the lithiation of the anode, the HCS tends to occupy the interfacial region, thus preventing some water molecules from contacting the anode surface (Figure 1b) and then generating a chemical environment that is more difficult for the HER.

To determine the optimal amount of TEAOTF added into the ACE, we performed Fourier-transform infrared spectroscopy (FTIR), Raman, and nuclear magnetic resonance (NMR). As shown in **Figure 2**a and Figure S1 (details in Note S1, Supporting Information), the FTIR and Raman spectra of ACE with TEAOTF reveal that the S–N–S bending vibration mode[5a,12] is nearly unchanged after adding 5 wt% TEAOTF. However, with TEAOTF increasing to 22 wt%, the S–N–S bending vibration mode exhibits a redshift of 2 cm−1. The same trend occurs in the C–F3 symmetric stretching mode, as shown in Figure 2b. These results suggest that 5 wt% TEAOTF does not change the chemical environment of anions, but the interaction between cations and anions becomes weaker as the TEAOTF increases from 5 to 22 wt%. In Figure 2c and Figure S2, the O–H stretching mode[13] of the water molecule remains constant before and after adding 5 wt% TEAOTF, indicating that the TEA+ cations are not solvated by water. By contrast, the O–H stretching mode exhibits a large redshift of 14 cm−1 for TEAOTF: 22 wt%, suggesting that excessive TEAOTF could affect the Li+–water solvation structure, weakening the interaction between water and salt. NMR measurements further confirm these results (Figure 2d–f). The 1H spectrum of water molecules exhibits nearly no change after adding 5 wt% TEAOTF, but there is a slight chemical shift of 0.09 ppm from 5 to 22 wt% TEAOTF (Figure 2d). A weaker electronic density is found around H and O of H2O in TEAOTF:22 wt% compared to TEAOTF:5 wt% (Figure 2d; Figure S3, Supporting Information). The 1H signals of CH3– and –(CH2)– verify the existence of TEA+ again (Figure 2d; Figure S4, Supporting Information). As shown in Figure 2e, with increasing TEAOTF, the 19F signals of TFSI− experience upfield shift of 0.02 (from 0 to 5 wt% TEAOTF) and 0.04 ppm (from 5 to 22 wt% TEAOTF), respectively, while the 19F signals of OTF− show a downfield shift of 0.14 ppm (from 5 to 22 wt% TEAOTF). This opposite trend for the 19F signals can be ascribed to the interaction of TEA+–TFSI− and TEA+–OTF−, demonstrating that the cation–anion interaction follows the order: TEA+–TFSI− > TEA+–OTF−. In ACEs with different amounts of TEAOTF, the 7Li signal shows an interesting upfield shift of 0.02 ppm from 0 to 5 wt% TEAOTF, indicating strong ion shielding or increased Lewis basicity around Li+ (Figure 2f).[13b] However, the 0.03 ppm downfield shift of 7Li signals from 5 to 22 wt% TEAOTF further verifies that the
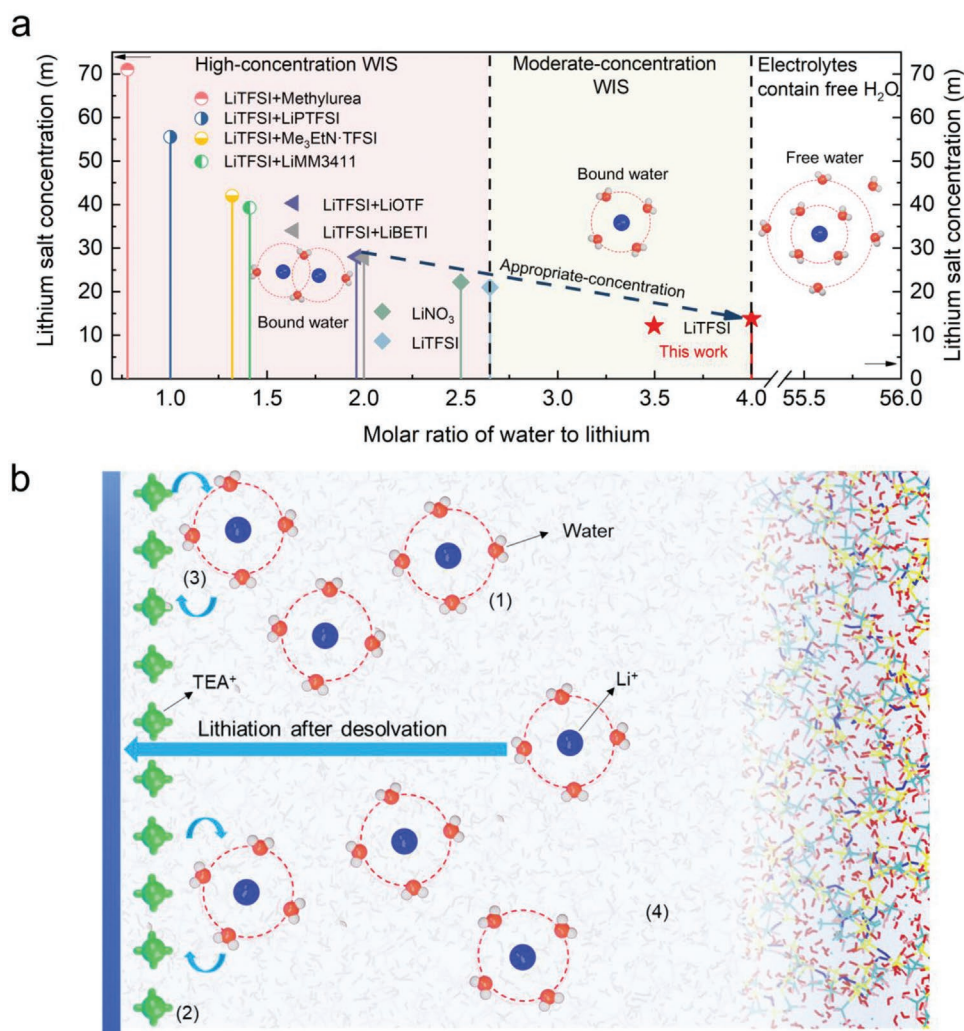
Figure 1. The interface construction of hydrophobic cationic sieve (HCS). a) Lithium salt concentration with the molar ratio of water to lithium.[1f,5a–c,7a–c] b) Schematics of HCS effect on the interfacial structure of anode. The labels in (b) indicate: (1) Bound water, (2) Hydrophobic cationic sieve (HCS), (3) Restrained HER, (4) Appropriate concentration electrolyte (ACE).

excessive addition of TEAOTF can damage the Li+–water solvation structure, which would enlarge the water activity.

FTIR, Raman, and NMR results were understood by MD simulations (Figure 2g; Table S1, Supporting Information). Specifically, the coordination number of TFSI− around TEA+ for TEAOTF:5 wt% is much more than that of OTF− (9.46 and 0.3, respectively; Figure 2h; Figure S5, Table S2 and Note S2, Supporting Information). This probably suggests that the general cation–anion interaction follows the order of TEA+–TFSI− > TEA+–OTF−, in line with our experimental observation. Moreover, OTF− shows a stronger interaction with Li+ than TFSI− (Table S3, Supporting Information) and then replaces TFSI− in the solvation shell of Li+ (Figures S6 and S7, Supporting Information). With the addition of TEAOTF, TFSI− associates less with Li+, thus obtaining a more negatively charged environment. The effect is opposite for OTF−, which is consistent with the ^{19}F shift trend observed for TFSI− and OTF− (Figure 2e). By scrutinizing the solvation shell of Li+ in different systems, we observe that the addition of TEAOTF decreases the coordination number of TFSI− and water

surrounding Li+ and increases that of OTF− (Figure 2i; Table S2, Supporting Information). Hence, the change of general charge around Li+ may vary with TEA+ concentration, which would account for the phenomenon in Figure 2f. Furthermore, with the addition of TEAOTF, the water staying in the solvation shell of Li+ changes very little with TEAOTF:5 wt%, while some water would become free for the TEAOTF:22 wt%, suggesting that adding 5 wt% TEAOTF will not effectively change the solvation structure of water (Figures S8 and S9, Supporting Information).

In short, it can be concluded that the optimum addition of TEAOTF is 5 wt%, which could achieve well-balanced interactions between Li+, water molecules, and anions. Herein, we define the ACE with 5 wt% TEAOTF as the HCS-ACE.

## 2.2. Modulating the Effect of the HCS on the Anode Interfacial Structure

To investigate how TEAOTF would affect the structure of electrode–electrolyte interfaces and then resist HER, MD
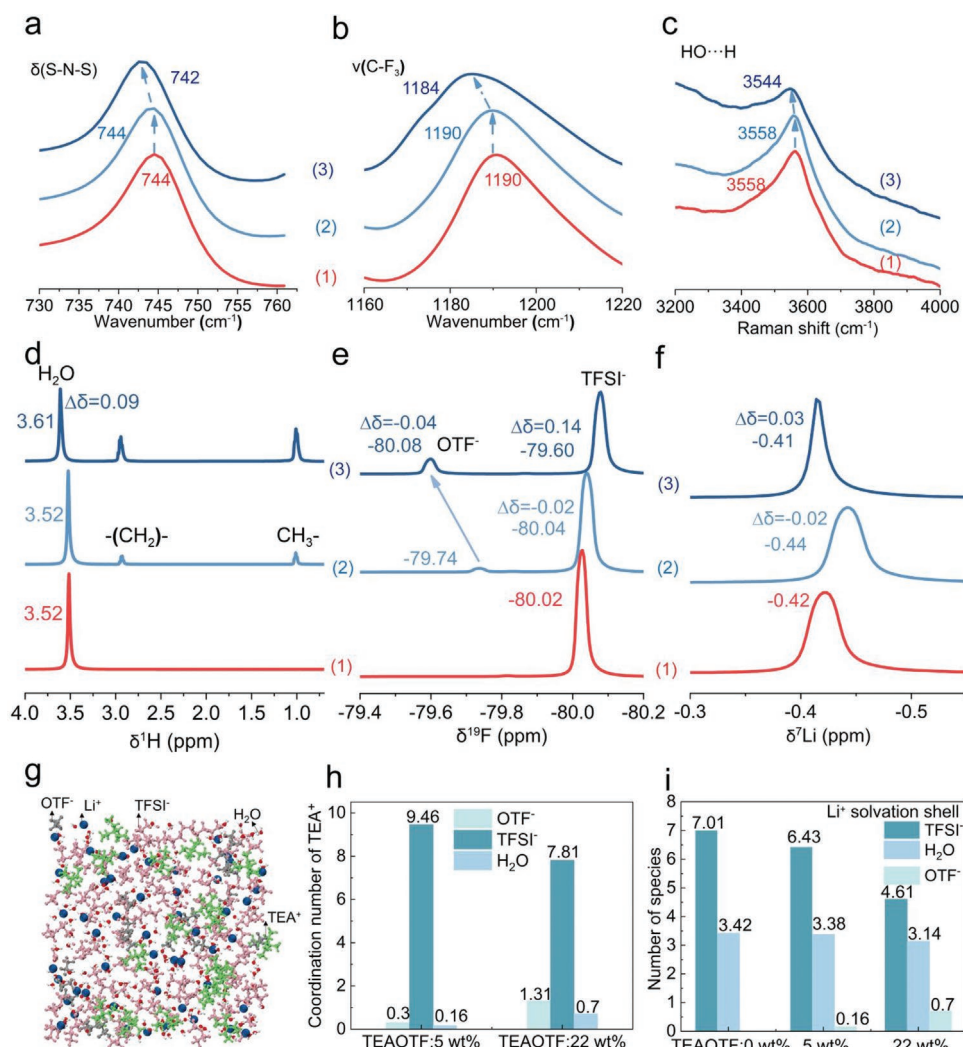
Figure 2. Cation–anion and ion–water interactions in ACE with the variation of TEAOTF. a) S–N–S bending vibration mode and b) C–F$_3$ symmetric stretching mode of ACE with 0, 5, and 22 wt% of TEAOTF in FTIR, denoted as: (1) TEAOTF: 0 wt%, (2) TEAOTF: 5 wt%, and (3) TEAOTF: 22 wt%, respectively. c) O–H stretching modes of water molecule of (1) TEAOTF: 0 wt%, (2) TEAOTF: 5 wt%, and (3) TEAOTF: 22 wt% in Raman. d) ^{1}H, e) ^{19}F, and f) ^{7}Li NMR chemical shift in: (1) TEAOTF: 0 wt%, (2) TEAOTF: 5 wt%, and (3) TEAOTF: 22 wt%. g) The snapshot of the MD simulation of TEAOTF: 5 wt%. h) the Coordination number of TEA$^+$ from MD simulation. i) Number of species of Li$^+$ solvation shell from MD simulation. The coordination number of other species is summarized in Table S2 (Supporting Information).

simulations of electrode–electrolyte interfaces were performed, constructed as the channel system (**Figure 3**a,b). With the addition of TEAOTF, the first peak of water number density decreases remarkably, regardless of the degree of negative polarization (Figure 3c,d; Figure S10, Supporting Information). The same trend is observed for Li$^+$ and TFSI$^-$. To quantitatively describe interfacial electrosorption, the accumulative number of each species in the interfacial region was calculated (Figure 3e,f; Figure S11, Supporting Information). With the addition of TEAOTF, interfacial water is reduced by 40%–50% (Figure 3e). Interfacial free water, which accounts for ≈10%–15% of the total interfacial water, is decreased by 20%–46% with adding TEAOTF (The details for the bound state of water are discussed in Note S2 and Figures S12–S14, Supporting Information). Despite the addition of a small amount of TEAOTF (the molar ratio of TEA$^+$ to Li$^+$ is 1:13.8; Table S1, Supporting Information), there is an adlayer of TEA$^+$ under 0 V (Figure 3c) with a strong van der Waals interaction with the anode (about −49 kJ mol^{-1},

Figure S15, Supporting Information), which is consistent with the free energy well below the bulk region (Figure S16, Supporting Information). The change of interfacial structure mainly caused by TEA$^+$ leads to a positive shift of point of zero charge (from −0.48 V for ACE to −0.35 V for HCE-ACE, taking bulk region in simulation system as reference), which is consistent with the experimental measurement (Figure S17, Supporting Information). As the polarization becomes more negative, the minimum value of free energy well decreases from −52.5 to −73.3 kJ mol^{-1} (Figure S16, Supporting Information) because of the enhanced electrostatic interaction (Figure S15, Supporting Information), leading to the stronger accumulation of TEA$^+$ ions on the anode (Figure 3f) and the formation of an electric-field-reinforced HCS that facilitates the exclusion of water at the anode. To find the origin of the decreased interfacial water via the HCS, we further explored the 2D structures of water and ions in the interfacial region. As shown in Figure 3g and Figures S18–S20, the water is in the vicinity of Li$^+$, consistent

ADVANCED
SCIENCE NEWS

www.advancedsciencenews.com

ADVANCED
MATERIALS

www.advmat.de
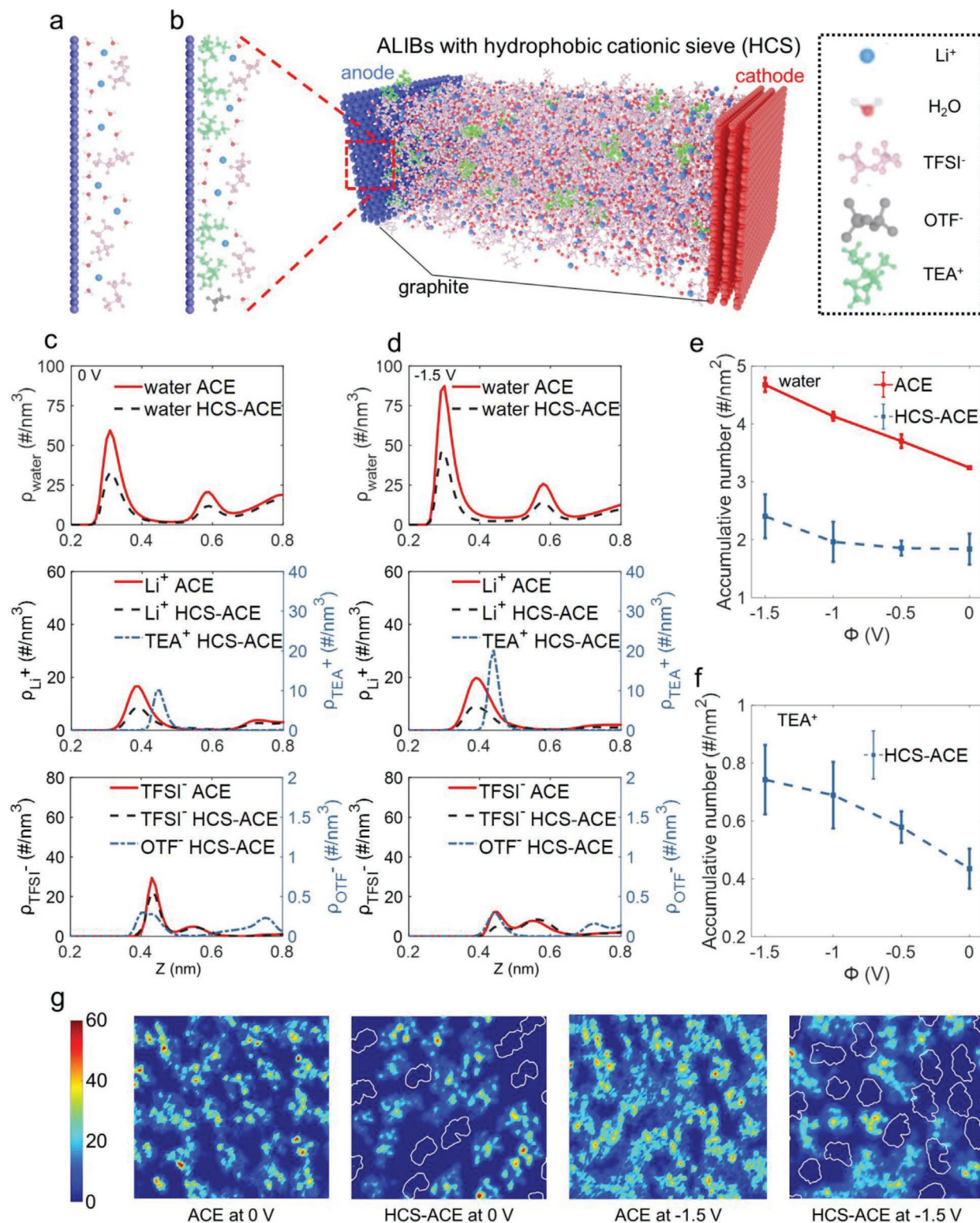
Figure 3. The interfacial structure at the anode. a) Interfacial structure without HCS. b) Snapshot of MD simulation containing HCS and the interfacial structure with HCS. c,d) Number density distribution of water (top), cations (middle), and anions (bottom) under potentials of 0 V (c) and −1.5 V (d). Throughout the analysis, the position of different species is based on the center of mass. e) Electrosorption of water at anode surface in ACE and HCS-ACE systems. The accumulative number was calculated by integrating number density in the interfacial region (0.35 nm from the anode, determined by water's vdW diameter[4e]). f) Electrosorption of TEA$^+$ at anode surface in HCS-ACE system. The accumulative number was calculated by integrating number density in the interfacial region (0.50 nm from the anode, which was determined based on the first valley of the number density distribution for TEA$^+$). g) 2D density distribution of interfacial water at the anode. The white lines sketch contours of HCS distribution. Unit of the color bar is # nm^{-3}.

**ADVANCED
SCIENCE NEWS**

www.advancedsciencenews.com

**ADVANCED
MATERIALS**

www.advmat.de

with that the majority of interfacial water molecules are bound with Li$^+$ (Figure S14, Supporting Information), while few water molecules stay in the space taken by hydrophobic TFSI$^-$. A considerable part of the interfacial space is occupied by the HCS after adding TEAOTF, and the room for interfacial water decreases remarkably (Figure 3g; Figures S18 and S21, Supporting Information). TEA$^+$, with four ethyl branches, shows the weakest interaction with water among the electrolyte components (Table S3, Supporting Information) and is large enough to achieve an effectual steric hindrance at the anode. Accordingly, fewer water molecules are found to stay within the interfacial region compared with the case in the absence of TEAOTF. The more negatively the anode is polarized, the larger is the amount of interfacial space occupied by TEA$^+$ cations, which leads to fewer interfacial water molecules (the decrease in interfacial water is 1.40 per nm^2 at 0 V and 2.27 per nm^2 under −1.5 V, Figure 3e). Therefore, the addition of TEA$^+$ modulates an interfacial microstructure with tougher kinetics for water touching the anode surface, which could potentially result in an environment wherein the HER is more difficult to occur. About the interfacial electrosorption of TEA$^+$ at cathode can be seen in Note S2 and Figure S22 (Supporting Information).
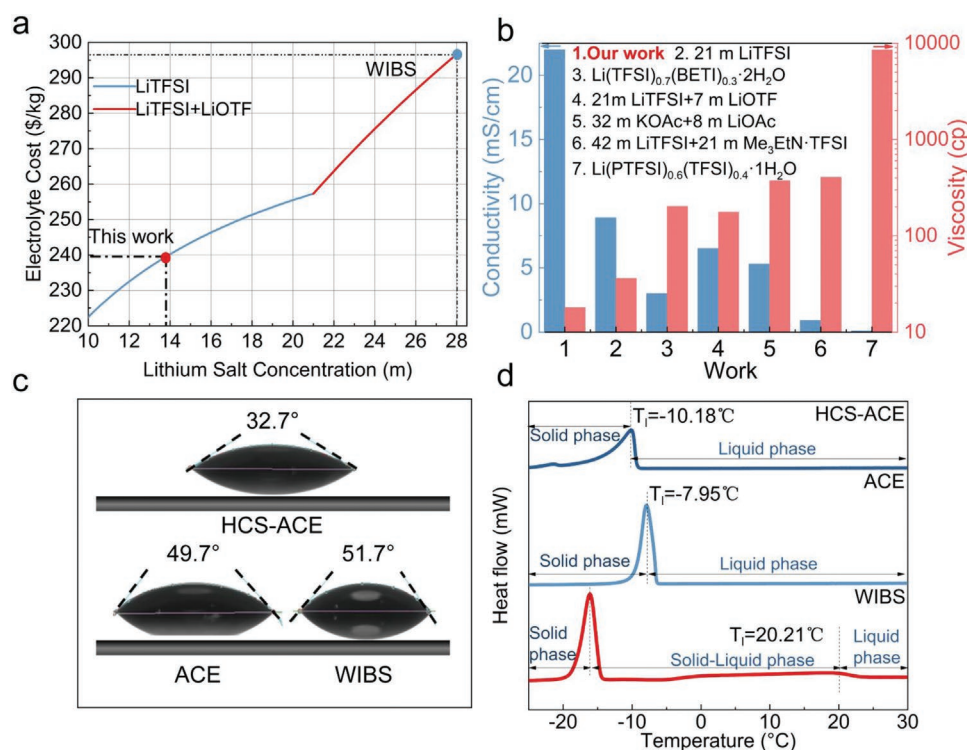
2.3. Physicochemical Properties of the HCS-ACE

Previous work has reported that WIBS (21 m LiTFSI + 7 m LiOTF) has a high cost due to its high concentration,[5b] whereas
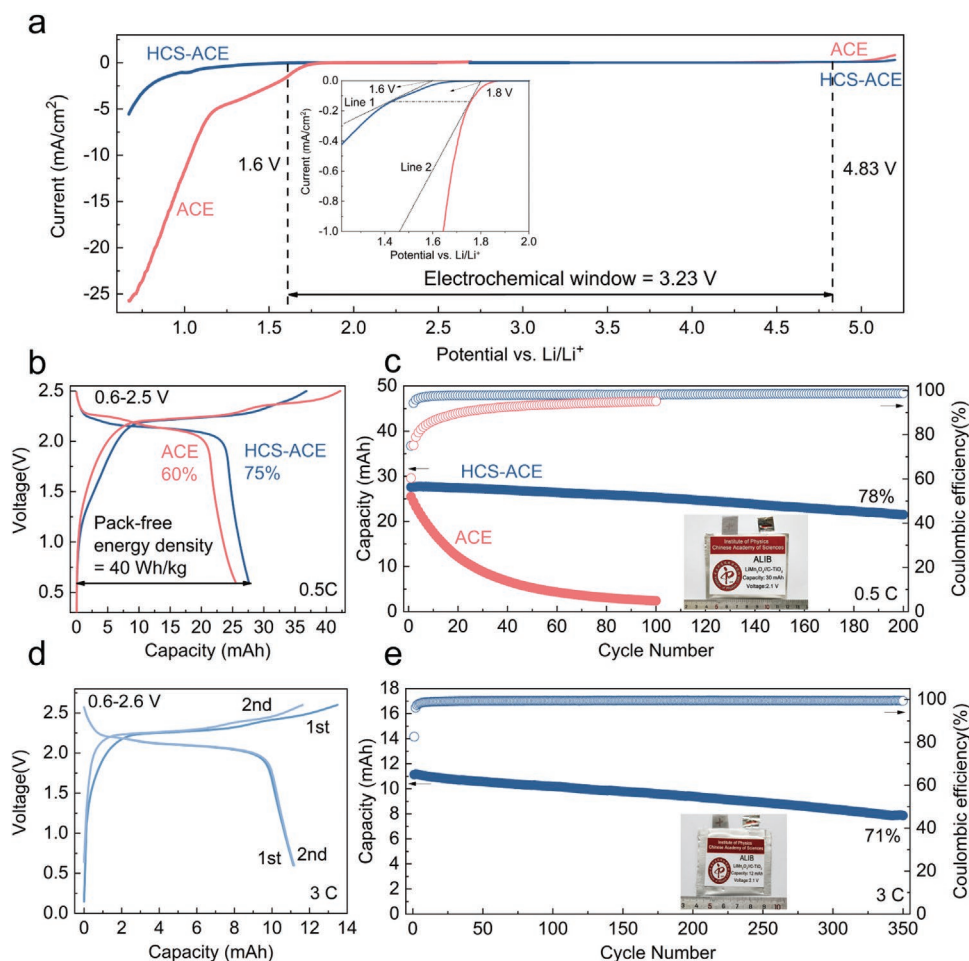
in this work, the proposed HCS-ACE has a much lower concentration, rendering a lower cost (**Figure 4**a; Note S3 and Table S4, Supporting Information). This decrease of lithium salt concentration brings out many advantages in ionic transport properties, including the highest ionic conductivity (22 mS cm^{-1} at 25 °C) and lowest viscosity (18 cP at 25 °C) among all available WIS electrolytes (Figure 4b; Table S5, Supporting Information). Furthermore, as a kind of surfactant, TEAOTF could effectively reduce the surface tension of water, thereby improving the wettability of electrolytes to the electrode.[14] As Figure 4c shows, the contact angle of HCS-ACE is 32.7°, demonstrating better wettability than ACE (49.7°) and WIBS (51.7°). Furthermore, the HCS-ACE exhibits a much lower solid–liquid transition temperature (T_l) of −10.18 °C compared to that of WIBS, which is 20.21 °C (Figure 4d; Figure S23, Supporting Information). Meanwhile, the HCS-ACE follows Arrhenius behavior at a wide temperature range of −20 to 20 °C, and WIBS displays an inflection point below −10 °C due to liquid–solid phase transition[15] (Figure S24, Supporting Information).

2.4. Evaluating the Electrochemical Power of the HCS-ACE

The electrochemical stability window of HCS-ACE and ACE was evaluated by linear sweep voltammetry (LSV) on the cathodic side (Al foil) and anodic side (Ti foil). Impressively, the electrochemical window of the HCS-ACE is measured to be 3.23 V (**Figure 5**a). It shows that the HER of HCS-ACE is

Figure 4. The physicochemical properties of HCS-ACE. a) Cost analysis between this work and WIBS. The price of LiTFSI is taken as 300 and 550 $ per kg for LiOTF (details in Experimental Section, Supporting Information). b) Comparison of ionic conductivity and viscosity for HCS-ACE, 21 m LiTFSI,[5a] Li(TFSI)$_{0.7}$(BETI)$_{0.3}$·2H$_2$O,[7a] 21 m LiTFSI + 7 m LiOTF,[5b] 32 m KOAc + 8 m LiOAc,[7e] 42 m LiTFSI + 21 m Me$_3$EtN·TFSI[7c] and Li(PTFSI)$_{0.6}$(TFSI)$_{0.4}$·H$_2$O[5c] electrolytes. c) The contact angles between the electrolyte of HCS-ACE, ACE, and WIBS. d) Thermal stability was measured by differential scanning calorimetry (DSC) at the rate of 2 °C min^{-1} from −25 to 30 °C of HCS-ACE, ACE, and WIBS. T_l means the liquid temperature.

ADVANCED
SCIENCE NEWS
www.advancedsciencenews.com

ADVANCED
MATERIALS
www.advmat.de

Figure 5. Electrochemical performance of HCS-ACE and ACE. a) The electrochemical window of ACE and HCS-ACE, which was measured on Al foil (cathodic side) and Ti foil (anodic side) at the scanning rate of 10 mV s^{-1}. Inset: onset of the HER potential of ACE and HCS-ACE. b) The first charge–discharge curves at 0.5 C (1 C = 168 mA g^{-1}) of 30 mAh (design capacity) pouch cell with ACE and HCS-ACE. The initial coulombic efficiency of the full cell with HCS-ACE and ACE is marked by the energy density of the full cell. c) The cycling performance and coulombic efficiency of 30 mAh pouch cell with ACE and HCS-ACE. Inset: Optical photograph of assembled 30 mAh ALIB pouch cell with HCS-ACE. d) The first and second charge–discharge curves at 3 C of 12 mAh (design capacity) pouch cell with HCS-ACE. e) The cycling performance and coulombic efficiencies of 12 mAh pouch cell. Inset: Optical photograph of assembled 12 mAh ALIB pouch cell with HCS-ACE. The mass ratio of cathode and anode in every pouch cell is 2.

significantly suppressed, compared with the ACE, and especially on the cathodic side, the potential can be defined as 1.6 V (inset of Figure 5a and details in Note S4, Supporting Information), which is lower than that of the ACE (1.8 V), illustrating that the small amount of TEA$^+$ can effectively suppress the HER and push the HER potential of 0.2 V. Even at challenging 1.0 V versus Li/Li$^+$,[5a,7c] the current density of HER in HCS-ACE (1.08 mA cm^{-2}) is an order of magnitude lower more than in ACE (11.7 mA cm^{-2}), which strongly proves the effective interfacial modulation of the HCS revealed by MD simulations. On the anodic side, the onset of oxygen evolution reaction (OER) potential is pushed from 4.78 V in ACE into 4.83 V in HCS-ACE (Figure S25 and Note S4, Supporting Information). The electrochemical stability window of ACE and HCS-ACE were also evaluated with a slow-scanning rate of 1 mV s^{-1}. The HER potential of HCS-ACE is 1.66 V, and the ACE is 2.01 V (Figure S26 and Note S4, Supporting Information). It is impressive that the HER potential of HCS-ACE is much lower than

that of ACE at a slow-scanning rate. In the interface environment without HCS, the HER reaction becomes more severe when the scan rate becomes lower (The HER potential of ACE is 1.8 V with 10 mV s^{-1} scanning rate, while The HER potential of ACE is 2.01 V with a 1 mV s^{-1} scanning rate. The HER potential of HCS-ACE is almost unchanged when the scanning rate becomes lower). This result strongly proves the effective interfacial modulation of the HCS revealed by MD simulations. Moreover, the small amount of TEA$^+$ not only changes the potential of HER but also reduces the H$_2$ evolution rate according to the Tafel slope in Figure S27 (The details in Note S4, Supporting Information). The onset of OER potential can be seen in Figure S26 and Note S4 (Supporting Information). The suppression of HER is further verified by cyclic voltammetry measurement (Figure S28, Supporting Information). A prominent reaction peak appears in ACE, while the curve remains the EDL behavior in HCS-ACE (Figure S28, Supporting Information). The electrochemical window of WIBS was measured. It

is worth noting that the HER potential of HCS-ACE is 1.60 V, which is comparable to that of WIBS. This result can prove again the ability of TEA$^+$ to suppress the HER (Figure S29 and Note S4, Supporting Information). Thus, with the support of the electric-field-reinforced HCS-ACE, the redox couple of spinel LiMn$_2$O$_4$ (LMO) and carbon-coated anatase TiO$_2$ (C-TiO$_2$) (see details in Figures S30–S32, Supporting Information), whose characteristic redox peaks are 4.55 V/4.22 V, 4.40 V/4.02 V, and 2.31 V/1.79 V, can be enveloped in the electrochemical window (Figure S33, Supporting Information). Moreover, the C-TiO$_2$ shows superior cycling reversibility in the half cell with a high mass loading condition of ≈11 mg cm^{-2} (Figure S34, Supporting Information).

Comparing the electrochemical windows of the ACE and HCS-ACE, it can be concluded that the electric-field-reinforced HCS could modulate the interfacial structure to significantly reduce the water at the anode interface, thereby shifting the negative potential of the HER. To demonstrate the electrochemical ability of HCS-ACE in the realistic full cell, we assembled the ALIBs with LMO cathode and C-TiO$_2$ anode. The full cell first processes 5 cycles at 5 C and then charges into 2.5 V, finally holding at 100% stage of charge (SOC) for 220 min to see the current decay (Figure S35, Supporting Information). It shows that the current decreases from 1.41 mA to less than 0.1 mA in 8 min, indicating the electrochemical stability of HCS-ACE. The self-discharge behavior of our ALIBs with HCS-ACE was evaluated in two methods shown in Figure S36 (Supporting Information). All the full cells with HCS-ACE were run at 2 C for 5 cycles first, then stood at the SOC of 100%. The full cells showed no obvious voltage drop after standing for 5000 min and can have 80% capacity retention after standing for 2000 min. It indicates a good storage performance of our full cells with HCS-ACE. Meanwhile, the in-situ pressure test with the cycling was conducted on our full pouch cell with HCS-ACE in Figure S37 (Supporting Information). It can be concluded that there is no noticeable change in pressure during cycling (the pressure is reduced by 6.86%), indicating that our full cell does not show obvious gas production during cycling. Also, our full cell with HCS-ACE and high mass loading LMO (≈20 mg cm^{-2}) and C-TiO$_2$ (≈11 mg cm^{-2}) demonstrate superior electrochemical performance with high-capacity retention and >99% Coulombic efficiency. These results can collectively illustrate the electrochemical stability of HCS-ACE. The electrochemical performance of the full cell in ACE with 22 wt% mentioned above was evaluated in Figure S38 (Supporting Information). The addition of 22 wt% TEAOTF significantly affects the electrochemical performance of the full cell probably due to the increase of free water.

Based on the above results, furthermore, the 2.5 V single-layer mAh-level pouch cell (design capacity: 30 mAh) with 2.1 V output voltage is constructed with LMO cathode (≈20 mg cm^{-2}) and C-TiO$_2$ anode (≈11 mg cm^{-2}) in a high mass loading condition. By sharp contrast, the ACE shows visible decomposition and low coulombic efficiency (the initial coulombic efficiency is 60% and stabilized to 95% after 100 cycles), resulting in the full cell that cannot survive beyond 100 cycles (Figure 5b,c). While benefiting from the electric-field-reinforced HCS, the full cell with HCS-ACE maintains higher coulombic efficiency of 75% initial efficiency and ≈99% after several cycles

(Figure S39, Supporting Information), which exhibits superior cycling stability with 78% capacity retention after 200 cycles at 0.5 C (Figure 5b,c). Because the HER and OER reactions[16] may not occur symmetrically in the aqueous batteries and the HER is easier to take place,[17] higher Coulombic efficiency indicates that the system has fewer HER and is more reversible. More importantly, our single-layer pouch cell (30 mAh) delivers 40 Wh kg^{-1} (note that the energy density calculation excludes the weight of the package,[18] and the details are listed in Table S6, Supporting Information). The 30 mAh pouch cell can maintain high energy efficiency (>85%, Figure S40, Supporting Information) during cycling, which is key to energy storage systems. Furthermore, the pouch cell with HCS-ACE shows a long-term cycle life of up to 350 cycles at 3.5 C with retention of 71% (Figure 5d,e). The XPS and TEM were performed on the C-TiO$_2$ electrode after cycling in HCS-ACE and found that no anion-derived SEI formed (Figures S41, S42 and Note S4, Supporting Information). The electric-field-reinforced HCS should be the critical factor for the superior performance of ALIBs with HCS-ACE.

The rate capability and low-temperature performance of HCS-ACE were evaluated in comparison with the WIBS. The full cell with HCS-ACE can release almost three times more capacity than that with WIBS at a low temperature of −20 °C, which illustrates superior low-temperature performance in HCS-ACE (**Figure 6**a). Meanwhile, the full cell displays outstanding rate capability, superior to WIBS (75.58% capacity retention at 4 C in HCS-WIS while 61.59% capacity retention at 4 C in WIBS, Figure 6b). The better temperature tolerance and rate capability of the full cell with the HCS-ACE originate from the higher ionic conductivity and lower solid–liquid transition temperature of the HCS-ACE compared with WIBS. Different from WIBS, which has higher T_1 (Figure 4d) and lower conductivity (0.44 mS cm^{-1} at −20 °C; Figure S22, Supporting Information) that result in poor kinetics at low temperature,[19] the HCS-ACE has a much lower T_1 (Figure 4d) and relatively higher conductivity at the same temperature (4.27 mS cm^{-1} at −20 °C; Figure S22, Supporting Information). The HCS-ACE has the profound advantages of high ionic transportation, low viscosity, and low liquid–solid transition temperature due to the decrease in lithium salt concentration. Noticeably, the full cell with the HCS-ACE can achieve a high-power density of 949 W kg^{-1} with remarkable cycling performance for 1000 cycles at 8 C with a capacity retention rate of almost 70% (Figure 6c). These results can be attributed to the better wettability, higher ionic conductivity, and lower viscosity of the HCS-ACE at room temperature. The full cells with WIBS were also evaluated at 0.5 and 8 C for long-term cycling performances for comparison shown in Figure S43 and Note S4 (Supporting Information). Meanwhile, the interfacial resistances of the full cell with HCS-ACE and WIBS were evaluated in Figure S44 (Supporting Information), showing better interfacial reaction kinetics of HCS-ACE than WIBS. To our knowledge, the electrochemical performance of LMO/TiO$_2$ can be the best with such dilute electrolyte in Table S7 (Supporting Information). Based on environmental friendliness, energy density, energy efficiency, cost, rate capability, and low-temperature performance, the figure of merit on ALIBs with HCS-ACE, ALIBs with concentrated electrolytes, and lead–acid batteries was draw (Figure 6d). Compared with
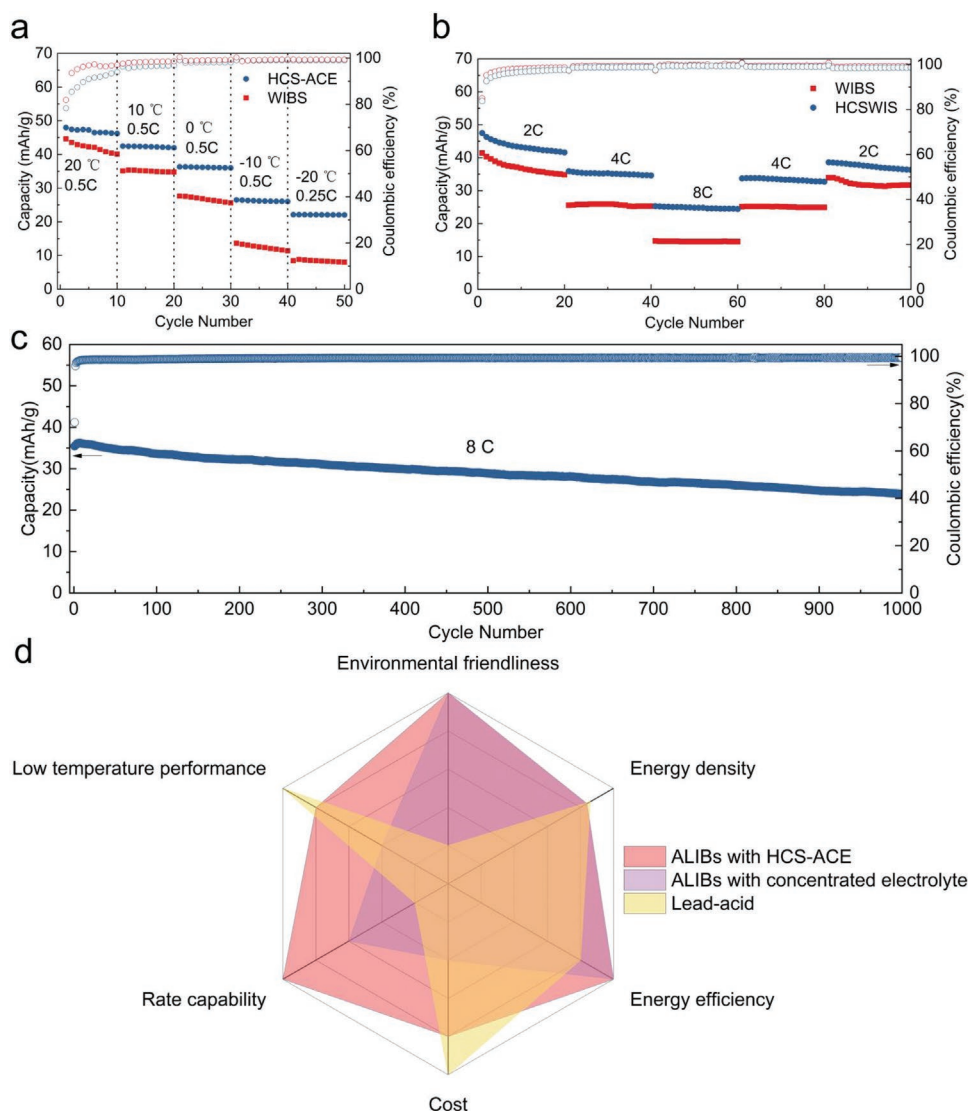
Figure 6. Rate capability and low-temperature performance of HCS-ACE. a) Electrochemical performance of the LMO/C-TiO$_2$ full cell at the low-temperature test from 20 to −20 °C in WIBS and HCS-ACE. b) Rate capability of the LMO/C-TiO$_2$ full cell of HCS-ACE and WIBS. c) Cycling performance of the LMO/C-TiO$_2$ full cell of HCS-ACE at a high rate of 8 C. The capacity is based on the mass of cathode and anode, the mass ratio of cathode and anode is 2. d) Figure of merit on ALIBs with HCS-ACE, ALIBs with concentrated electrolytes, and lead–acid batteries.

ALIBs with concentrated electrolytes, the ALIBs with HCS-ACE have better low-temperature performance, better rate capability, and lower cost. Compared with lead–acid batteries,[17a] the ALIBs with HCS-ACE are more environmentally friendly with better rate capability and higher energy density.

3. Conclusion

We have proven the importance of the conceptional HCS for the stability of aqueous electrolytes, which can reduce high-concentration electrolytes to an ACE. Our simulations suggest that the introduction of TEA$^+$ can modulate the interface structure at the anode. As a large hydrophobic cation, TEA$^+$ can be absorbed on negatively polarized electrodes to form HCS, occupying parts of the interfacial space at the anode. Thus, owing

to the hydrophobic nature of TEA$^+$, some water molecules are excluded from the interfacial region and have difficulty contacting the anode surface. This contributes to an environment wherein it is more difficult for the HER to occur. Moreover, when the electrode polarization becomes more negative, more TEA$^+$ ions can accumulate at the anode, and more water molecules are expelled from the anode interface, implying that the HCS effect is electric-field-reinforced. The wider stable electrochemical window of HCS-ACE indicates the restraint of the HER at the anode interface. Compared with the ACE, a full cell with the HCS-ACE achieves better cycling performance (78% retention after 200 cycles at 0.5 C in mAh-level pouch cell), higher coulombic efficiency (≈99% at 0.5 C), and high energy density (40 Wh kg^{-1}). Meanwhile, owing to the decrease in concentration, the HCS-ACE possesses high ionic conductivity and a low liquidus temperature. Therefore, a full cell with the

HCS-ACE has better rate performance and low-temperature performance than with WIBS. Our work provides an essential step toward developing high-performance and low-cost ALIBs for large-scale energy storage and a fundamental understanding of interfacial chemistries in ALIBs.

This work also demonstrates that the sizable hydrophobic cation plays an essential role in adjusting the anode interface structure to suppress the HER in aqueous electrolytes. This strategy could be extended to other large cations, like asymmetric trimethylpropyl$^+$ (TMP$^+$) and symmetric tetrabutylammonium$^+$ (TBA$^+$), with different structures and sizes. Importantly, our work reveals that ALIBs with decreased lithium salt concentration of aqueous electrolytes and low-cost electrode materials, such as $LiMn_2O_4$ and anatase TiO_2, are suitable for large-scale energy storage and sustainable aqueous batteries.

4. Experimental Section

The details of experimental section/methods are in the Supporting Information.

Supporting Information

Supporting Information is available from the Wiley Online Library or from the author.

Conflict of Interest

The authors declare no conflict of interest.

Data Availability Statement

The data that support the findings of this study are available from the corresponding author upon reasonable request.

[1] a) W. Li, J. R. Dahn, D. S. Wainwright, *Science* **1994**, *264*, 1115; b) J. Y. Luo, W. J. Cui, P. He, Y. Y. Xia, *Nat. Chem.* **2010**, *2*, 760; c) J. Xie, Z. Liang, Y. C. Lu, *Nat. Mater.* **2020**, *19*, 1006; d) Y. Zhao, Z. Chen, F. Mo, D. Wang, Y. Guo, Z. Liu, X. Li, Q. Li, G. Liang, C. Zhi, *Adv. Sci.* **2021**, *8*, 2002590; e) D. Chao, W. Zhou, F. Xie, C. Ye, H. Li, M. Jaroniec, S.-Z. Qiao, *Sci. Adv.* **2020**, *6*, eaba4098; f) R. Lin, C. Ke, J. Chen, S. Liu, J. Wang, *Joule* **2022**, *6*, 399; g) M. Turgeman, V. Wineman-Fisher, F. Malchik, A. Saha, G. Bergman, B. Gavriel, T. R. Penki, A. Nimkar, V. Baranauskaite, H. Aviv, M. D. Levi, M. Noked, D. T. Major, N. Shpigel, D. Aurbach, *Cell Rep. Phys. Sci.* **2022**, *3*, 100817.

[2] C. Wessells, R. Ruffo, R. A. Huggins, Y. Cui, *Electrochem. Solid-State Lett.* **2010**, *13*, A59.

[3] a) A. Zhou, Y. Liu, X. Zhu, X. Li, J. Yue, X. Ma, L. Gu, Y.-S. Hu, H. Li, X. Huang, L. Chen, L. Suo, *Energy Storage Mater.* **2021**, *42*, 438; b) C. Yang, J. Chen, T. Qing, X. Fan, W. Sun, A. von Cresce, M. S. Ding, O. Borodin, J. Vatamanu, M. A. Schroeder, N. Eidson, C. Wang, K. Xu, *Joule* **2017**, *1*, 122.

[4] a) J. Vatamanu, O. Borodin, *J. Phys. Chem. Lett.* **2017**, *8*, 4362; b) M. McEldrew, Z. A. H. Goodwin, A. A. Kornyshev, M. Z. Bazant, *J. Phys. Chem. Lett.* **2018**, *9*, 5840; c) G. Feng, X. Jiang, R. Qiao, A. A. Kornyshev, *ACS Nano* **2014**, *8*, 11685; d) C. Y. Li, J. B. Le, Y. H. Wang, S. Chen, Z. L. Yang, J. F. Li, J. Cheng, Z. Q. Tian, *Nat. Mater.* **2019**, *18*, 697; e) M. Chen, J. Wu, T. Ye, J. Ye, C. Zhao, S. Bi, J. Yan, B. Mao, G. Feng, *Nat. Commun.* **2020**, *11*, 5809; f) X. Shan, D. S. Charles, Y. Lei, R. Qiao, G. Wang, W. Yang, M. Feygenson, D. Su, X. Teng, *Nat. Commun.* **2016**, *7*, 13370.

[5] a) L. M. Suo, O. Borodin, T. Gao, M. Olguin, J. Ho, X. L. Fan, C. Luo, C. S. Wang, K. Xu, *Science* **2015**, *350*, 938; b) L. M. Suo, O. Borodin, W. Sun, X. L. Fan, C. Y. Yang, F. Wang, T. Gao, Z. H. Ma, M. Schroeder, A. von Cresce, S. M. Russell, M. Armand, A. Angell, K. Xu, C. S. Wang, *Angew. Chem., Int. Ed.* **2016**, *55*, 7136; c) S. Ko, Y. Yamada, K. Miyazaki, T. Shimada, E. Watanabe, Y. Tateyama, T. Kamiya, T. Honda, J. Akikusa, A. Yamada, *Electrochem. Commun.* **2019**, *104*, 106488; d) M. Wang, S. Liu, H. Ji, T. Yang, T. Qian, C. Yan, *Nat. Commun.* **2021**, *12*, 3198.

[6] a) C. Y. Yang, X. Ji, X. L. Fan, T. Gao, L. M. Suo, F. Wang, W. Sun, J. Chen, L. Chen, F. D. Han, L. Miao, K. Xu, K. Gerasopoulos, C. S. Wang, *Adv. Mater.* **2017**, *29*, 8; b) L. M. Suo, F. D. Han, X. L. Fan, H. L. Liu, K. Xu, C. S. Wang, *J. Mater. Chem. A* **2016**, *4*, 6639; c) C. Yang, J. Chen, X. Ji, T. P. Pollard, X. Lü, C.-J. Sun, S. Hou, Q. Liu, C. Liu, T. Qing, Y. Wang, O. Borodin, Y. Ren, K. Xu, C. Wang, *Nature* **2019**, *569*, 245.

[7] a) Y. Yamada, K. Usui, K. Sodeyama, S. Ko, Y. Tateyama, A. Yamada, *Nat. Energy* **2016**, *1*, 9; b) J. Forero-Saboya, E. Hosseini-Bab-Anari, M. E. Abdelhamid, K. Moth-Poulsen, P. Johansson, *J. Phys. Chem. Lett.* **2019**, *10*, 4942; c) L. Chen, J. Zhang, Q. Li, J. Vatamanu, X. Ji, T. P. Pollard, C. Cui, S. Hou, J. Chen, C. Yang, L. Ma, M. S. Ding, M. Garaga, S. Greenbaum, H.-S. Lee, O. Borodin, K. Xu, C. Wang, *ACS Energy Lett.* **2020**, *5*, 968; d) Y. Yamada, J. Wang, S. Ko, E. Watanabe, A. Yamada, *Nat. Energy* **2019**, *4*, 269; e) M. R. Lukatskaya, J. I. Feldblyum, D. G. Mackanic, F. Lissel, D. L. Michels, Y. Cui, Z. Bao, *Energy Environ. Sci.* **2018**, *11*, 2876; f) X. He, B. Yan, X. Zhang, Z. Liu, D. Bresser, J. Wang, R. Wang, X. Cao, Y. Su, H. Jia, C. P. Grey, H. Frielinghaus, D. G. Truhlar, M. Winter, J. Li, E. Paillard, *Nat. Commun.* **2018**, *9*, 5320.

[8] S. Yang, F. Zhang, H. Ding, P. He, H. Zhou, *Joule* **2018**, *2*, 1648.

[9] a) L. M. Suo, D. Oh, Y. X. Lin, Z. Q. Zhuo, O. Borodin, T. Gao, F. Wang, A. Kushima, Z. Q. Wang, H. C. Kim, Y. Qi, W. L. Yang, F. Pan, J. Li, K. Xu, C. S. Wang, *J. Am. Chem. Soc.* **2017**, *139*, 18670; b) X. Wu, Y. Xu, C. Zhang, D. P. Leonard, A. Markir, J. Lu, X. Ji, *J. Am. Chem. Soc.* **2019**, *141*, 6338.

[10] a) S. Banerjee, X. Han, V. S. Thoi, *ACS Catal.* **2019**, *9*, 5631; b) S. Banerjee, Z.-Q. Zhang, A. S. Hall, V. S. Thoi, *ACS Catal.* **2020**, *10*, 9907; c) F. Wang, C.-F. Lin, X. Ji, G. W. Rubloff, C. Wang, *J. Mater. Chem. A* **2020**, *8*, 14921; d) N. Dubouis, A. Serva, R. Berthin,

G. Jeanmairet, B. Porcheron, E. Salager, M. Salanne, A. Grimaud, *Nat. Catal.* **2020**, *3*, 656.

[11] I. Persson, *Pure Appl. Chem.* **2010**, *82*, 1901.

[12] I. Rey, P. Johansson, J. Lindgren, J. C. Lassègues, J. Grondin, L. Servant, *J. Phys. Chem. A* **1998**, *102*, 3249.

[13] a) L. Jiang, Y. Lu, C. Zhao, L. Liu, J. Zhang, Q. Zhang, X. Shen, J. Zhao, X. Yu, H. Li, X. Huang, L. Chen, Y.-S. Hu, *Nat. Energy* **2019**, *4*, 495; b) N. Dubouis, P. Lemaire, B. Mirvaux, E. Salager, M. Deschamps, A. Grimaud, *Energy Environ. Sci.* **2018**, *11*, 3491.

[14] L. L. Schramm, E. N. Stasiuk, D. G. Marangoni, R. S. C. Rsc, *Annu. Rep. Prog. Chem., Sect. C: Phys. Chem.* **2003**, *99*, 3.

[15] a) O. Borodin, L. M. Suo, M. Gobet, X. M. Ren, F. Wang, A. Faraone, J. Peng, M. Olguin, M. Schroeder, M. S. Ding, E. Gobrogge, A. V. Cresce, S. Munoz, J. A. Dura, S. Greenbaum, C. S. Wang, K. Xu, *ACS Nano* **2017**, *11*, 10462; b) G. Perron, D. Brouillette, J. E. Desnoyers, *Can. J. Chem.* **1997**, *75*, 1608.

[16] Y. Dou, T. Liao, Z. Ma, D. Tian, Q. Liu, F. Xiao, Z. Sun, J. Ho Kim, S. Xue Dou, *Nano Energy* **2016**, *30*, 267.

[17] a) L. Droguet, A. Grimaud, O. Fontaine, J. M. Tarascon, *Adv. Energy Mater.* **2020**, *10*, 2002440; b) D. Strmcnik, M. Uchimura, C. Wang, R. Subbaraman, N. Danilovic, D. van der Vliet, A. P. Paulikas, V. R. Stamenkovic, N. M. Markovic, *Nat. Chem.* **2013**, *5*, 300.

[18] a) L. Lin, K. Qin, Q. Zhang, L. Gu, L. Suo, Y. S. Hu, H. Li, X. Huang, L. Chen, *Angew. Chem. Int. Ed. Engl.* **2021**, *60*, 8289; b) J. Betz, G. Bieker, P. Meister, T. Placke, M. Winter, R. Schmuch, *Adv. Energy Mater.* **2018**, *9*, 1803170.

[19] Q. Zhang, Y. Ma, Y. Lu, L. Li, F. Wan, K. Zhang, J. Chen, *Nat. Commun.* **2020**, *11*, 4463.